Deep electron and hole polarons and bipolarons in amorphous hafnium oxide

Moloud Kaviani,[1,*] Jack Strand,[2,†] Valery V. Afanas'ev,[3,‡] and Alexander L. Shluger[4,2,§]

[1] *Advanced Institute for Materials Research (AIMR), Tohoku University, Sendai 980-8577, Japan*
[2] *Department of Physics and Astronomy and London Centre for Nanotechnology, University College London, Gower Street, London WC1E 6BT, United Kingdom*
[3] *Department of Physics, University of Leuven, Celestijnenlaan 200D, 3001 Leuven, Belgium*
[4] *Advanced Institute for Materials Research (AIMR),Tohoku University, Sendai 980-8577, Japan*

Using both classical and *ab initio* calculations we show that excess electrons and holes can trap in amorphous hafnium oxide (a-HfO_2) structures in deep band gap states. Amorphous hafnia models were generated using classical force-fields and their geometries optimised using density functional theory (DFT). Calculations of the geometrical and electronic structures of excess electrons and holes demonstrate that they localize spontaneously at precursor sites, such as longer Hf–O bonds or under-coordinated Hf atoms. Single electron polarons produce states in the gap at ∼2 eV below the bottom of the conduction band with average trapping energies of 1.0 eV. Two electrons can form bipolarons creating even deeper states below the bottom of the conduction band. Holes are typically localized on two under-coordinated O ions with average trapping energies of 1.3 eV.

Although self-trapping of small electron and hole polarons is common it is usually shallow in crystalline oxides, with trapping energies of the order of 0.2 eV. The electron and hole polarons are mobile at room temperature in crystalline reduced TiO_2 and NiO [1], CeO_2 [2, 3], doped ZrO_2 [4, 5], and in plethora of other oxides (see e.g. [6–10]). The intrinsic localization of excess electrons and holes in non-crystalline materials and liquids has also been a subject of experimental and theoretical studies over the last 70 years [11]. Structural disorder induces shallow electron states near the bottom of the conduction band, below the so-called mobility edge (see, for example, [12]).

Recent results suggest that intrinsic electron and hole localisation in deep states is also possible in some amorphous oxides, where electrons and holes either do not self-trap or form only shallow states in the crystalline phase of the material. In amorphous SiO_2, holes [13] and electrons have been shown [14, 15], to localize spontaneously in deep states with well-defined EPR and optical absorption signatures measured experimentally [16]. Trapping energies of holes in amorphous TiO_2 have been calculated to be much larger than these in rutile [17]. Under-coordinated indium has been suggested to act as a deep intrinsic electron-trap center in amorphous $InGaZnO_4$ by theoretical calculations [18]. In these systems, the polaronic relaxation is amplified by the local disorder of amorphous network. Here we demonstrate by theoretical modelling that both electrons and holes can trap spontaneously in deep states induced by the reduced coordination and disorder of network atoms (with trapping energies exceeding 1.0 eV) in amorphous (a)-HfO_2. Moreover, electrons also form even deeper bipolaron states, which have not been observed before in binary oxides.

In recent years HfO_2 based insulators emerged as the primary contenders to replace SiO_2 in a broad spectrum of nano-electronic devices ranging from deep-scaled transistors to DRAM and non-volatile memory cells (see, e.g. [19, 20]). Small polaron electron an hole mobility has been observed in n-doped ZrO_2 [4, 5], which is isostructural and has very similar properties to HfO_2. Shallow electron and hole polaron states in crystalline monoclinic (m)-HfO_2 and ZrO_2 have been predicted by theoretical calculations [21]. Subsequent work [22] confirmed that holes can self-trap at three-coordinated O sites in m-HfO_2 and ZrO_2 with trapping energies of about 0.2 eV and in much deeper states at some low-coordinated O sites at the surface of ZrO_2 [23]. Recent resonant photoelectron spectroscopy measurements strongly suggest hole polaron trapping in HfO_2 thin films [24]. Accumulation of negative charge associated with deep electron trapping states observed in amorphous HfO_2 films [25] has not yet been understood. More generally, amorphous oxides make the backbone of most electronic devices and charge trapping and carrier mobility are very important in all these applications.

Previous results demonstrate that disorder and local coordination clearly play important roles in creating deep states for polaron localization. However, HfO_2 is not a conventional glass former and forms amorphous structures in thin films due to the deposition process and substrate constraints. These films often become polycrystalline during anneal above 450 °C (see e.g. [26]). Models of a-HfO_2 structures are usually obtained using a melt-quench procedure similar to that used to create a-SiO_2 structures [18, 27–30]. In this work we used this method and classical molecular dynamics accompanied by the structure relaxation using energy minimization and Density Functional Theory (DFT). LAMMPS package [31] was used with two different force-fields: relatively simple pair potentials (PP) parametrized in [27] and a more complex charge equilibration force-field COMB [32] for comparison. In all cases, cubic periodic cells were initially equilibrated at 300 K and constant pressure of 1 atm. The temperature was then linearly ramped to 6000 K at constant pressure and the structures were sta-

bilized for 500 ps at 6000 K. The systems were cooled down from 6000 K to 0 K in 8 ns with a cooling rate of 0.75 K.ps^{-1}. The Berendsen thermostat and barostat were used to control the temperature during the simulations. In spite of relatively slow cooling rate comparing to other studies, these structures essentially correspond to frozen melt.

TABLE I. Distribution of O and Hf ion coordination numbers in a-HfO_2 with different sizes. Coordination numbers fractions are in percentage.

Kind	CN	96	324	768	1500	6144
Hf	5	8.1	9.6	9.0	9.7	8.2
	6	47.6	65.6	78.1	75.5	75.3
	7	44.3	24.8	12.9	14.8	16.5
O	2	6.4	6.0	6.1	6.6	5.8
	3	69.2	83.1	85.9	84.3	84.2
	4	24.4	10.9	8.0	9.1	10.0

Both types of forcefields produce samples with densities of about 9.0 g cm^{-3}. Amorphous structures exhibit wide distributions of bond lengths and atomic coordinations. The coordination number of each atom was determined by counting the number of atoms within a cut-off radius of 2.35 Å. Since periodic boundary conditions impose constraints, we checked the dependence of the structure on the cell size. The results for different cell sizes presented in Table 1 demonstrate the convergence for cell sizes exceeding 324 atoms. They are in qualitative agreement with other theoretical studies [30, 33, 34] and importantly do not depend significantly on the force-field used. The structures generated by the COMB force-field are very close to those produced by the activation relaxation technique [35] at the same density. We note that detailed quantitative comparison with previous studies is hampered by the fact that melt-quench methods use very different cooling rates and either predict or use different densities (ranging between 8.6 and 10.6 g cm^{-3} for HfO_2). Nevertheless, all calculations show the existence of two-coordinated O and five-coordinated Hf ions, which are important for our further predictions. We note that the distribution of ionic coordinations is the main difference with the a-SiO_2 structure where the local coordination of Si and O ions is largely preserved. Similar behaviour has been observed in other glass structures which do not contain typical network-forming cations [18, 36].

Studying the statistical distributions of properties of polarons requires extensive quantum mechanical calculations, which restrict the maximum cell size to 324 atoms. We have run exploratory calculations in 96 atom cells accompanied by further calculations in 324 atom cells. Thirty four periodic models with 96 atoms and 9 models with 324 atoms in a cell were created using PP for this purpose. Ten 96 and 324 atom models were created using the same procedure and the COMB force-field to check the dependence of the results on the forcefield used.

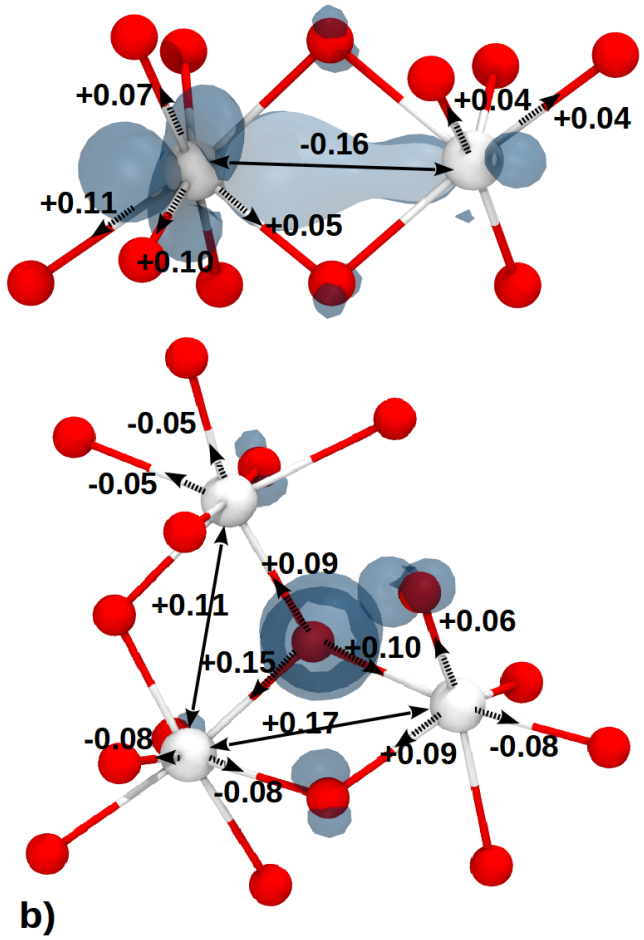

FIG. 1. The displacements of the Hf and O atoms caused by the localization of the extra electron and hole in a-HfO_2. The arrows show the direction of displacements. a) Atomic displacements around an electron trapping site; and b) atomic displacements around a hole trapping site. Displacements less than 0.03 Å have not been shown. The dashed arrows show bond length and solid arrows show distance changed between two atoms from the neutral values. All numbers are in Å. The yellow bubbles are the visualisation of the spin density of the trapped electron. Different iso-value has been used for clarity. The white spheres are Hf atoms and the red spheres are O atoms.

Further optimization of the volume and geometry of these structures was performed using DFT implemented in the CP2K code [37, 38] with the non-local PBE0-TC-LRC functional and the exchange cutoff radius of 4.0 Å [38]. The CP2K code employs a Gaussian basis set mixed with an auxiliary plane-wave basis set [39]. The double-ζ Gaussian basis-sets[40] were employed on all atoms in conjunction with the GTH pseudopotential [41]. The plane-wave cutoff was set to 6530 eV (480 Ry). To reduce the computational cost of nonlocal functional calculations, the auxiliary density matrix method (ADMM)

was employed [38]. All geometry optimizations were performed using the BFGS optimizer to minimize forces on atoms to within 2.3×10^{-2} eV Å^{-1}. The trapping energies of excess electrons and holes are corrected using the method of Lany and Zunger [42, 43]. The average value of a single localized charge correction for 34 structures with 96-atom a-HfO_2 supercells is 0.05 eV.

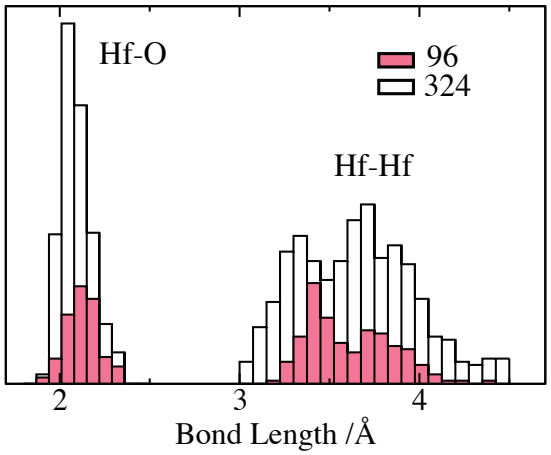

FIG. 2. Histogram of the Hf–O and Hf–Hf bond lengths.

The DFT geometry optimization of the volume and atomic structures obtained using classical MD calculations does not change the topology of a-HfO_2 models. However, the optimized structures have higher densities, in the range of 9.2-9.9 g cm^{-3}, averaging at 9.6 g cm^{-3}. The wide distributions of Hf−O and Hf−Hf bond lengths obtained after DFT cell and geometry optimization of neutral cells are illustrated in Fig. 2. The average Hf–O bond length is 2.1 Å (ranging from 1.95 to 2.35 Å) is very close to the Hf–O bond lengths in m-fO_2 (around 2.1 Å). In further calculations we compare the characteristics of excess electrons and holes in 96 and 324 atom structures having similar densities in the range of 9.6-9.7 g cm^{-3} and across the whole density range.

Calculations of the electron trapping in m-HfO_2 show no electron localization and predict hole spontaneous self-trapping only at 3-coordinated oxygen sites with trapping energy of 0.5 eV. The latter is calculated as the total energy difference between the delocalized hole state in the perfect lattice and the fully relaxed hole state.

Electron trapping in a-HfO_2 was explored first using 34 periodic models of a-HfO_2 containing 96 atoms and then tested further using 324 atom cells. The electronic structure calculations predict an average band gap of ∼6.4 eV for 96 atom cells and ∼6.0 eV for 324 atom cells, ranging between 5.8 and 6.2 eV, which is in good agreement with the experimental data [24]. To study the electron trapping, an extra electron was first added to these models and the geometry of each system was optimized. We observe spontaneous electron localization in deep states in each system. Unlike m-HfO_2, the electron initially is not completely delocalized over the entire system, but exhibits preferential localization on some Hf atoms forming a precursor state. For example, in the structure shown in Figure 1a the excess electron is initially localized on two Hf atoms to 7% and 18% whereas the rest of the spin density is delocalized over other Hf atoms. After the geometry relaxation, the electron localization on these two Hf atoms increases to 21% and 60%, respectively. Further analysis of precursor sites demonstrates that in 60% cases the extra electron is localized on the hafnium atoms which have at least three oxygen neighbors with the distance longer than 2.16 Å. In around 32% of the cases the extra electron is localized by the five- coordinated hafnium atoms. These Hf atoms also have longer Hf–O bonds. In some rare cases (∼8%) the extra electron is trapped on Hf atoms forming wide O–Hf–O angles and elongated Hf–O bonds.

More than 80% of the electron spin density is localized predominantly on two or three Hf ions sharing a three coordinated oxygen atom. Out of our 34 structures, in 24 models the extra electron is localized on two neighboring Hf atoms shearing at least a three coordinated oxygen atom. In 7 models the extra electron is localized on three Hf atoms and in 4 models the extra electron is localized on 4 Hf atoms. The spin density is usually distributed non-homogeneously among these Hf atoms and the rest of the spin density is delocalized over other Hf atoms. The geometry optimization exposes a strong structural distortion of the Hf–Hf and Hf–O bonds around the electron localization site (see Fig. 1a). Typically, the Hf atoms with the localized electron displace closer (by around 0.20 Å) to each other. In addition, the electron localization leads to Hf–O bond weakening so that the Hf–O bonds become longer on average by around 0.12 Å. We note that both the character of electron localization and the local network distortion around the electron trapping site are qualitatively similar to those found for an electron polaron and negatively charged vacancy in m-HfO_2 the extra electron is localized by two or three Hf atoms with one of them bearing most of the spin density [21]. However, the trapping energy and the Kohn-Sham levels in the gap are much deeper in the amorphous structure.

The electron trapping energies calculated as total energy differences between the initial electron state in amorphous structure and after the geometry optimization average at ∼ 0.77 eV with a wide distribution ranging between 0.54 eV and 1.07 eV. These energies give a lower limit to thermal ionization energies of trapped electrons and suggest that most of these electrons will be stable at room temperature. The average position of the KS level, from the 34 models of 96 atoms, is 2.07 eV, ranging from ∼ 1.3 eV to 2.75 eV below the bottom of the conduction band (CB), indicating a deep electron trap. Thus the first excess electron digs a deep potential well in the amorphous structure.

It turns out that this well can accommodate two paired

electrons forming a bipolaron. The second electron is localized at the same place with a similar pattern of network distortion, making the Hf-O bonds longer by ∼0.09 Å and the Hf–Hf distance shorter by ∼0.14 Å. This network relaxation facilitates creation of a deeper singlet KS state in the gap at ∼2.24 eV, ranging from 1.4 to 3.4 eV below the bottom of the conduction band. For some of the structures this level is around 1.1 eV deeper compared to the single-electron trap. This trend is similar to the bipolaron trapping in another ionic system - alkali halide melts [44–46]. It stems from the fact that the relaxation energy accompanying the second electron localization is comparable to that for the first electron due to the low density of a-HfO_2, but the kinetic energy increase due to the second electron localization is much smaller as it is initially well localised in the potential well.

We used the same approach to study hole trapping in a-HfO_2. The trapping of hole polarons on single O atoms in m-HfO_2 has been previously predicted theoretically [21]. Recent calculations using the cancellation of nonlinearity approach [47] predicted that holes can trap only at 3-coordinated O sites in the bulk of m-HfO_2 [22] with trapping energy of 0.18 eV and with much larger trapping energies at surfaces, featuring 2-coordinated O sites.

We find hole localization in all 34 models of a-HfO_2. The energy minimisation with respect to the initial state causes a distortion in the amorphous network and leads to localisation of over 90% of the hole spin density over two O atoms. The distribution over the two oxygens is, however, not equal with the hole occupying predominantly one O atom. The characteristic atomic displacements accompanying the hole localization are shown in Fig. 1b. The average hole trapping energy is 0.61 eV, ranging between 0.39 eV and 0.98 eV. These values are close to those found for hole trapping at different surface sites of m-HfO_2 [23]. The latter is not particularly surprising as precursor sites for the hole localization are 2-coordinated O atoms in amorphous network.

To expose other hole localization sites, we also investigated the effect of inserting two holes into our amorphous cells. In the singlet state, neither one of the holes trap and both remain within delocalised states in the valence band. In the triplet state, both holes are localized on different O sites, that is, we do not see bi-hole traps. The structural distortions predicted here are mostly the same as in the single hole trapping case, with the exception that some structures see more exaggerated structure distortion (the oxygen atom gets displaced by between 0.3 to 0.8 Å) and larger trapping energies of, on average, 1.5 eV. This results from the interference of distortion regions created by each hole in the amorphous network.

We used 324-atom cells to check the effect of the cell size on the network relaxation around the electron trapping site and to reduce the periodic image interaction. The average position of the KS level for the electron polaron in these structures is 2.10 eV ranging from 1.63 to 2.38 eV below the bottom of conduction band with an average trapping energy of 1.0 eV, ranging from 0.5 to 1.15 eV. The average position of the KS level for bipolaron is 1.93 eV, ranging from 1.10 to 2.60 eV below the bottom of conduction band. The average hole trapping energy is also increased to 1.3 eV mainly due to the larger number of atoms involved in the network distortion in a bigger cell. We also find that 324-atom cells contain up to four precursor sites for both electron and hole trapping with trapping energies distributed within about 0.8 eV. We assume that they become randomly populated by injected electrons or holes and therefore give the total distribution of trapping energies and positions of KS levels rather than these corresponding to the lowest energy states.

To summarize, we have generated models of amorphous HfO_2 with a range of densities using two different force-fields and a melt-quench method and investigated electron and hole localization in these models. The results demonstrate that both electrons and holes can localize in a-HfO_2 in deep states with the trapping energies much larger than those predicted in m-HfO_2. A bipolaron localization is predicted in deeper states than for single electrons. Excess electrons are localized typically on two or three Hf ions associated with longer Hf–O bonds or under-coordinated Hf atoms in the structures and induce strong polaronic distortion of the surrounding network. The hole trapping takes place predominantly at 2-coordinated O sites.

The broad distribution of the one-electron levels with respect to the bottom of the CB exhibits two maxima at 2.0 eV and 2.5 eV, corresponding to single- and bi-electron traps. These energies depend on the a-HfO_2 density and on the local environment of trapping sites. For the experimental density of 9.6 g cm^{-3}, they are in good agreement with the experimental data [25, 48] where exhaustive photo-depopulation spectroscopy was used to determine the energy distribution of tapped electrons in HfO_2 layers prepared using different Hf precursors or subjected to the post-deposition anneal. These measurements identified two kinds of intrinsic deep electron traps in amorphous HfO_2 films energetically distributed at 1.5 - 3.0 eV below the oxide CB bottom edge at room temperature.

These results demonstrate that excess electrons and holes localize in crystalline and amorphous HfO_2 in a qualitatively similar manner, but trapping energies in amorphous structures can be much larger. They broaden the concept of intrinsic polaron trapping to disordered wide gap oxides. Localization of excess electrons in deep states has so far been observed in a small number of systems, such as polar [49, 50] and non-polar [51, 52] liquids, ammonia and water ice and amorphous films on metal substrates [53–55], and alkali halide melts [44, 45, 56, 57]. In the latter case, bi-polarons facilitated by fluctuations

in the melt have also been observed and calculated [44–46], although electron polarons do not form in alkali halide crystals.

Our results may also have profound implications for our understanding of charge trapping in functional ceramics. The polaron states in the gap of a-HfO_2 are close to the position of the bottom of Si conduction band at Si/HfO_2 interface indicating that these states can be populated via direct tunnelling or via electron injection in the oxide. Similar states may exist in other amorphous oxide films and nanoparticles, such as Al_2O_3, ZrO_2, and TiO_2 [17].

MK and ALS are grateful to the World Premier International Research Center Initiative (WPI) sponsored by the Ministry of Education, Culture, Sports, Science and Technology (MEXT), Japan for financial support. JS is funded by EPSRC. VVA and ALS thank the EU FP7 project MORDRED (EU Project grant No. 261868) and COST Action CM1104 for financial support. Computer facilities on Archer service have been provided via the UKs HPC Materials Chemistry Consortium, which is funded by EPSRC (EP/F067496). The authors wish to thank Al-Moatasem El-Sayed, David Z. Gao, Thomas Durrant, Kazuto Akagi for helpful discussions and Adam Foster and Tiziana Musso for help in using COMB forcefield in LAMMPS.

* moloud.kaviani@gmail.com
† jack.strand.14@ucl.ac.uk
‡ valeri.afanasiev@fys.kuleuven.be
§ a.shluger@ucl.ac.uk

[1] I. Austin and N. Mott, Advances in Physics **50**, 757 (2001).
[2] H. Tuller and A. Nowick, Journal of Physics and Chemistry of Solids **38**, 859 (1977).
[3] I. Naik and T.-Y. Tien, Journal of Physics and Chemistry of Solids **39**, 311 (1978).
[4] W. Weppner, Zeitschrift für Naturforschung A **31**, 1336 (1976).
[5] J.-H. Park and R. N. Blumenthal, Journal of the Electrochemical Society **136**, 2867 (1989).
[6] A. Bosman and H. Van Daal, Advances in Physics **19**, 1 (1970).
[7] O. Schirmer, in *Defects and Surface-Induced Effects in Advanced Perovskites* (Springer, 2000) pp. 75–88.
[8] A. Stoneham, J. Gavartin, A. Shluger, A. Kimmel, G. Aeppli, C. Renner, *et al.*, Journal of Physics: Condensed Matter **19**, 255208 (2007).
[9] A. S. Alexandrov and J. T. Devreese, *Advances in polaron physics* (Springer, 2010).
[10] A. J. Rettie, W. D. Chemelewski, D. Emin, and C. B. Mullins, The journal of physical chemistry letters (2016).
[11] H. Frohlich, in *Proceedings of the Royal Society of London A: Mathematical, Physical and Engineering Sciences*, Vol. 188 (The Royal Society, 1947) pp. 521–532.
[12] N. Mott, Journal of Physics C: Solid State Physics **20**, 3075 (1987).
[13] D. L. Griscom, Journal of non-crystalline solids **352**, 2601 (2006).
[14] A.-M. El-Sayed, M. B. Watkins, V. V. Afanas' ev, and A. L. Shluger, Physical Review B **89**, 125201 (2014).
[15] A. El-Sayed, K. Tanimura, and A. Shluger, Journal of Physics: Condensed Matter **27**, 265501 (2015).
[16] Y. Sasajima and K. Tanimura, Physical Review B **68**, 014204 (2003).
[17] H. H. Pham and L.-W. Wang, Physical Chemistry Chemical Physics **17**, 541 (2015).
[18] H.-H. Nahm and Y.-S. Kim, NPG ASIA MATERIALS **6** (2014).
[19] M. Houssa, *High k Gate Dielectrics* (CRC Press, 2003).
[20] G. He and Z. Sun, *High-k Gate Dielectrics for CMOS Technology* (John Wiley & Sons, 2012).
[21] D. M. Ramo, A. Shluger, J. Gavartin, and G. Bersuker, Physical review letters **99**, 155504 (2007).
[22] K. P. McKenna, M. J. Wolf, A. L. Shluger, S. Lany, and A. Zunger, Physical review letters **108**, 116403 (2012).
[23] M. J. Wolf, K. P. McKenna, and A. L. Shluger, The Journal of Physical Chemistry C **116**, 25888 (2012).
[24] S. Alberton Corrêa, S. Brizzi, and D. Schmeißer, (2016).
[25] V. V. Afanas' ev, W. C. Wang, F. Cerbu, O. Madia, M. Houssa, and A. Stesmans, ECS Transactions **64**, 17 (2014).
[26] Y. Zheng, S. Wang, and C. Huan, Thin solid films **504**, 197 (2006).
[27] G. Broglia, G. Ori, L. Larcher, and M. Montorsi, Modelling and Simulation in Materials Science and Engineering **22**, 065006 (2014).
[28] D. Vanderbilt, X. Zhao, and D. Ceresoli, Thin Solid Films **486**, 125 (2005).
[29] Y. Wang, F. Zahid, J. Wang, and H. Guo, Physical Review B **85**, 224110 (2012).
[30] T.-J. Chen and C.-L. Kuo, Journal of Applied Physics **110**, 064105 (2011).
[31] S. Plimpton, Journal of computational physics **117**, 1 (1995).
[32] T.-R. Shan, B. D. Devine, J. M. Hawkins, A. Asthagiri, S. R. Phillpot, S. B. Sinnott, *et al.*, Physical Review B **82**, 235302 (2010).
[33] S. Clima, Y. Chen, R. Degraeve, M. Mees, K. Sankaran, B. Govoreanu, M. Jurczak, S. De Gendt, and G. Pourtois, Applied Physics Letters **100**, 133102 (2012).
[34] R. Ramprasad and C. Tang, in *APS Meeting Abstracts*, Vol. 1 (2010) p. 24004.
[35] D. Ceresoli and D. Vanderbilt, Physical Review B **74**, 125108 (2006).
[36] J. Akola, S. Kohara, K. Ohara, A. Fujiwara, Y. Watanabe, A. Masuno, T. Usuki, T. Kubo, A. Nakahira, K. Nitta, *et al.*, Proceedings of the National Academy of Sciences **110**, 10129 (2013).
[37] J. VandeVondele, M. Krack, F. Mohamed, M. Parrinello, T. Chassaing, and J. Hutter, Computer Physics Communications **167**, 103 (2005).
[38] M. Guidon, J. Hutter, and J. VandeVondele, Journal of Chemical Theory and Computation **5**, 3010 (2009).
[39] B. G. LIPPERT, J. H. PARRINELLO, and MICHELE, Molecular Physics **92**, 477 (1997).
[40] J. VandeVondele and J. Hutter, The Journal of chemical physics **127**, 114105 (2007).
[41] S. Goedecker, M. Teter, and J. Hutter, Phys. Rev. B **54**, 1703 (1996).
[42] S. Lany and A. Zunger, Modelling and Simulation in Ma-

terials Science and Engineering **17**, 084002 (2009).
[43] S. Lany and A. Zunger, Physical Review B **78**, 235104 (2008).
[44] B. Von Blanckenhagen, D. Nattland, K. Bala, and W. Freyland, The Journal of chemical physics **110**, 2652 (1999).
[45] O. Terakado, P. Poh, and W. Freyland, Journal of Physics: Condensed Matter **15**, 1553 (2003).
[46] E. Fois, A. Selloni, M. Parrinello, and R. Car, The Journal of Physical Chemistry **92**, 3268 (1988).
[47] S. Lany and A. Zunger, Physical Review B **81**, 205209 (2010).
[48] V. Afanasev and A. Stesmans, Journal of applied physics **95**, 2518 (2004).
[49] Y. Tang, H. Shen, K. Sekiguchi, N. Kurahashi, T. Mizuno, Y.-I. Suzuki, and T. Suzuki, Physical Chemistry Chemical Physics **12**, 3653 (2010).
[50] S. C. Doan and B. J. Schwartz, The journal of physical chemistry letters **4**, 1471 (2013).
[51] B. Yakovlev, Russian Chemical Reviews **48**, 615 (1979).
[52] W. Schmidt and E. Illenberger, Nukleonika **48**, 75 (2003).
[53] R. Balog, P. Cicman, D. Field, L. Feketeova, K. Hoydalsvik, N. C. Jones, T. A. Field, and J.-P. Ziesel, The Journal of Physical Chemistry A **115**, 6820 (2011).
[54] J. Stähler, U. Bovensiepen, M. Meyer, and M. Wolf, Chemical Society Reviews **37**, 2180 (2008).
[55] J. Stähler, M. Meyer, U. Bovensiepen, and M. Wolf, Chemical Science **2**, 907 (2011).
[56] H. Brands, N. Chandrasekhar, H. Hippler, and A.-N. Unterreiner, Physical Chemistry Chemical Physics **7**, 3963 (2005).
[57] S. Dogel, W. Freyland, H. Hippler, D. Nattland, C. Nese, and A.-N. Unterreiner, Physical Chemistry Chemical Physics **5**, 2934 (2003).